Published in final edited form as:
Ultrasound Med Biol. 2007 March ; 33(3): 472–482.

Evaluating Thin Compression Paddles for Mammographically Compatible Ultrasound

Rebecca C. Booi[1,2], **Jochen F. Krücker**[1], **Mitchell M. Goodsitt**[1], **Matthew O'Donnell**[2], **Ajay Kapur**[3], **Gerald L. LeCarpentier**[1], **Marilyn A. Roubidoux**[1], **J. Brian Fowlkes**[1], and **Paul L. Carson**[1,2]

1 *Dept of Radiology, University of Michigan Ann Arbor, MI, 48109 USA*

2 *Biomedical Engineering Dept. University of Michigan Ann Arbor, MI, 48109 USA*

3 *General Electric Global Research Center Niskayuna, NY, 12309 USA*

Abstract

We are developing a combined digital mammography/3D ultrasound system to improve detection and/or characterization of breast lesions. Ultrasound scanning through a mammographic paddle could significantly reduce signal level, degrade beam focusing, and create reverberations. Thus, appropriate paddle choice is essential for accurate sonographic lesion detection and assessment with this system. In this study, we characterized ultrasound image quality through paddles of varying materials (lexan, polyurethane, TPX, mylar) and thicknesses (0.25–2.5 mm). Analytical experiments focused on lexan and TPX, which preliminary results demonstrated were most competitive. Spatial and contrast resolution, sidelobe and range lobe levels, contrast and signal strength were compared with no-paddle images. When the beamforming of the system was corrected to account for imaging through the paddle, the TPX 2.5 mm paddle performed the best. Test objects imaged through this paddle demonstrated ≤ 15% reduction in spatial resolution, ≤ 7.5 dB signal loss, ≤ 3 dB contrast loss, and range lobe levels ≥ 35 dB below signal maximum over 4 cm. TPX paddles < 2.5 mm could also be used with this system, depending on imaging goals. In 10 human subjects with cysts, small CNR losses were observed but were determined to be statistically insignificant. Radiologists concluded that 75% of cysts in through-paddle scans were at least as detectable as in their corresponding direct-contact scans. (Email: rbooi@umich.edu)

Keywords

3D imaging; Sonography; Quality assessment; Breast; Multimodality

Introduction

Breast ultrasound examinations are currently performed free-hand by a radiologist or a technician as a supplement to mammography when lesions are radiographically suspicious or indeterminate. These ultrasound images correspond to a different imaging geometry than the mammograms and, for at least 10% of the time, there is a discrepancy between the lesions detected with the two modalities (Conway et al. 1991). A combined x-ray/ultrasound system

Corresponding Author: Rebecca Booi, 200 Zina Pitcher Pl, 3315 Kresge III, Ann Arbor, MI 48109 USA, Phone Number: (734) 936-0195, Fax Number: (734) 764-8541, Email: rbooi@umich.edu

essentially eliminates this problem by first taking a digital x-ray over a compressed breast, then scanning a high frequency (9–12 MHz) ultrasonic transducer across the mammographic paddle while the breast is still under compression. This creates x-ray and ultrasound images in the same imaging geometry. The resulting 3D full field-of-view ultrasound images can later be registered to the digital mammograms. Thus this method of scanning might be able to expand the utility of ultrasound breast imaging and replace some hand-held, direct-contact ultrasound.

Sonographic detection of cancer has been problematic because it has relied heavily on operator and interpreter skill and patience. False positives are a particular problem when searching for secondary masses and for detection in high risk or screening populations. When supplemental to mammography, however, ultrasound has been a valuable tool in detecting and characterizing lesions in asymptomatic high-risk women, including those with mammographically dense breasts (Taylor et al. 2002;Moss et al. 1999;Lister et al. 1998;Stavros et al. 1995;Jackson et al. 1993;Bassett and Kimme-Smith 1991;Jackson 1990). Concurrent screening with these two imaging modalities using high quality equipment and performed by a skilled physician is reported to inexpensively provide high mammographic-US correlation of breast lesions and to significantly improve cancer detection (Novak 1983;Kolb et al. 1998;Brem and Gatewood 1992; Lunt et al. 1991).

Other systems developed for ultrasound imaging of a compressed breast through a mammographic paddle have experienced limited success (Schütze et al. 1998;Richter 1997;Richter 1995;Richter 1994;Moskalik et al. 1995;Kelly-Fry and Jackson 1991). Some of the difficulties that these systems faced included highly attenuating compression paddles, substantial reverberations, low frequencies, weakly focused beams and image artifacts created by refractions through the paddles. By thoroughly evaluating compression paddles to find nearly ideal material(s) and thickness(es) for both mammographic and sonographic requirements, we hope to improve on these past efforts.

Dual-mode whole-breast imaging also exhibits significant potential for advanced x-ray and ultrasound modes which would provide additional information about breast tissues that is not available from conventional ultrasound and mammography. For example, x-ray tomosynthesis could substitute digital mammography in the combined system for 3D delineation of tissue structures. In particular, we are targeting two advanced ultrasound modes - color flow Doppler and elasticity imaging – to assess both their fit with the system and their ability to provide supplemental physiological and mechanical information about breast tissues. Collectively, these techniques could provide radiologists with a more complete evaluation of breast tissue, improving the fidelity of lesion detection and characterization.

The goal of the present study was to compare image quality of the combined system (automated, through-paddle scanning) with that of current practice (hand-held, direct-contact scanning). Ultrasound image quality of the combined system could be adversely affected in comparison with direct-contact ultrasound because of three key factors.

First, the compression paddle affects the point- or line-spread function (PSF or LSF) of the system by refracting and attenuating the ultrasound beam. This refraction then exacerbates reverberation artifacts. Thus, the primary focus of this study was to investigate the consequences of imaging through the paddle on the LSF, sidelobe levels, range lobes (reverberations), contrast and signal loss. Some of these effects can be partly compensated by modifying the beamforming of the ultrasound scanner (Hoctor and Thomenius 2003,Krücker et al. 2004). The efficacy of such corrections and severity of remaining differences compared with direct-contact scanning were evaluated in several test object experiments and on human subjects examined with known cysts.

In addition, parallel compression paddles may introduce acoustic coupling difficulties on the sides of the breast and in the areolar region. Preliminary methods to increase breast contact with the paddle are introduced in this study and suggestions for other techniques to improve contact are addressed.

Finally, the probe with holder restricts access to parts of the breast, such as those near the chest wall. Scanning through a paddle limits insonification angles and planes, which could impede visualization of specular surfaces and increase the possibility that shadows from Coopers ligaments obstruct other tissue visibility. Imaging at 20° or in trapezoidal mode could lessen these issues. This paper did not evaluate image quality under those conditions, but initial images are shown in Figure 7 and are addressed further in the Conclusions section.

Methods

Experimental Set-up

Human subject experiments were conducted at the Cancer and Geriatric Center at the University of Michigan Medical Center on the combined system using a GE Logiq 9 scanner and GE Senographe 2000D digital mammography unit (Figure 1a). Test object experiments were performed on the stand-alone (ultrasound only) modified dual system developed by researchers at the University of Michigan and General Electric (GE Health Systems, Milwaukee, WI, USA). All experiments used a 1.5D M12L array transducer (length = 39 mm, focus = 1.6 cm) operating at 10 MHz. It was housed in a carriage and attached to two motors translating it across the mammographic paddle (Figure 1b). The transducer carriage was spring-loaded to ensure constant contact with the paddle. Hardware and software were developed for both systems to semi-automatically drive the transducer across the compression paddle, as well as to communicate with the Logiq 9 ultrasound system to trigger image and data acquisition (Kapur et al. 2004).

Choice of Mammographic Compression Paddles

Standard mammography compression paddles are 2.5 mm thick and made of lexan, a polycarbonate. However, the high level of acoustic attenuation in lexan (23.2 dB/cm at 5 MHz) precludes this standard mammographic paddle from sonographic imaging. Simply reducing paddle thickness insufficiently solves this problem, since a thin paddle will excessively deform under the pressure required to compress the breast, resulting in a non-planar scanning surface. Another option then is to investigate alternative paddle materials with improved sonographic imaging characteristics.

Mammographic paddles used with the combined system should have favorable mechanical, x-ray, optical and acoustical properties. A paddle should be mechanically tough and rigid, bowing less than 1 cm when maximum allowed force (200 N) is applied (FDA 1997). It should be uniform mammographically and acoustically as well as relatively transparent mammographically, acoustically, and optically. The preferred paddle would have an acoustic impedance that is well matched with both breast tissue (~1.5 kg/m^2s) and the transducer lens to minimize reverberations and beam refraction. These properties are further discussed in Kapur et al. (2004).

The paddle materials and thicknesses chosen for this study have a combination of the above mentioned mammographic and acoustic characteristics and are commercially available. They are: TPX (a polymethylpentene) 0.25, 0.5, 1.0 and 2.5 mm thick, lexan 125, 250 and 375 μm thick, mylar (a polyester) 250 μm thick and polyurethane 500 μm thick. Preliminary results revealed that only TPX and lexan materials were acoustically competitive for use with this

system, so this report will directly compare the TPX 2.5 mm and lexan 375 μm paddles. The acoustic properties of these two materials are listed in Table 1.

Beamforming Corrections

Most ultrasound scanners compute the electronic time delays used for focusing the ultrasound beam and scan-converting the received echo by treating tissue as a one-layer system with a fixed speed of sound (c = 1.54 mm/μs). However, the speeds of sound of most paddle materials are significantly greater than that of tissue. Thus, the propagation of the ultrasound beam through the mammographic paddle causes the beam to deviate from its assumed path, displacing it off the focus of the transducer. These aberrations can deteriorate image contrast and resolution, degrading diagnostic value. To compensate, time-delay corrections were applied to take into account the speed of sound through the mammographic paddle. Treating the paddle as an additional propagation layer with a distinct speed of sound, beam refraction occurs at the entrance and exit of the layer, behaving according to Snell's Law. Since the position of the layer is known, computation of the corresponding phase delays follows the approach described in further detail by Krücker et al. (2004). Corrections were not implemented in the elevational direction, because their effect would be minimal due to the transducer's small aperture size and number of independent elements in that direction.

Test Object Experiments

Test objects were chosen to measure those aspects of image quality predicted to degrade as a result of imaging through a mammographic paddle, mainly image resolution and contrast. These test objects are described below, and were used to select preferred paddle materials and thicknesses for the combined system. These results were then confirmed *in vivo* by imaging patients with simple cysts.

A step-shaped string test object was constructed to evaluate the space-varying LSF, as shown in Figure 2a. Steps were designed such that the LSF of each of the twenty 25 μm silver strings did not interfere with each other and so the LSF could be determined at a number of discrete depths from 3–40 mm from the transducer face. The test object was immersed in a tank of saline at body temperature (c = 1.54 mm/μs). Saline also provided acoustic coupling between the transducer and paddle except when the paddle was not deep enough to contain liquid, in which case ultra-myossage lotion (Chattanooga Medical Supply, Chattanooga, TN, USA) was used instead. Sound absorbing rubber surrounded the line targets to eliminate extraneous reverberations. To avoid saturation of pixel amplitudes caused by the low attenuation of saline, a preliminary experiment was conducted on the targets to determine the appropriate gain to utilize the full dynamic range without saturating.

The space-varying LSFs were measured in the lateral (along the length of the array), axial (perpendicular to the array face) and elevational (out of plane) directions. To determine lateral and axial LSFs, the test object was turned so the length of the transducer was perpendicular to the length of the strings. Lateral LSFs were constructed at each discrete depth by plotting a horizontal line through the center of each string cross-section displayed in the resulting image. Analogously, axial LSFs were constructed at each discrete lateral position by plotting a vertical line through the center of each string cross-section. The elevational extent between the strings was too great for all of them to appear in a single image. Therefore, to obtain the elevational LSF at each discrete depth, the transducer was positioned parallel to the length of the strings and scanned in 100 μm increments over a 5 cm elevational distance. Twenty-one adjacent y–z (elevational-axial) planes were extracted from the center of this volume and the peak value over this range was selected to account for small string fluctuations in the saline. Then, the elevational LSF was constructed by plotting a horizontal line through each string in this final image.

The spatial resolution of the system was determined from the LSF using the measures of full-width at half-maximum (FWHM, −6 dB) and full-width at tenth-maximum (FWTM, −20 dB). Pixel amplitudes were log-decompressed to dB values from a log-linear grayscale map according to the equation for the "E" grayscale curve setting on the scanner:

$$Y = [20\log_{10}(X + 1)] * \frac{255}{DR}, \quad (1)$$

where the first half of the equation converts pixel amplitude to dB and the second half of the equation scales these dB values by the number of gray scale levels (255) divided by the dynamic range (DR), 72 dB, in all experiments. This high DR was chosen to accommodate the large differences in signal level seen in breasts, from anechoic cysts to bright glandular tissue.

Main sidelobe levels and range lobe amplitudes, which include all reverberations, relative to maximum signal were calculated in the elevational and axial directions, respectively. Errors due to electronic noise were minimized by fitting these values to spatial polynomials of appropriate degrees. Each paddle's axial and lateral LSF was measured with and without beamforming corrections.

To measure contrast, a contrast-detail test object (Computerized Imaging Reference Systems, Norfolk, VA, USA (CIRS), Model 47) was imaged. This object contained an anechoic cylinder which was angled along the length of the test object relative to the transducer. To simulate a small simple cyst occurring at a range of depths, the transducer was translated over this object for 80 mm in step sizes of 500 μm. The contrast between the spherical cross-section of the cylinder (diameter = 2.4 mm) and the test object background was the calculated as a function of depth. In each acquired image, the center of the cylinder was manually identified and then three circles with radii 1.2 mm, 2.2 mm and 4.2 mm were drawn from that center, as shown in Figure 2b. The mean amplitude in the anechoic cylinder was calculated in the innermost circle. The mean amplitude of the background was calculated in the area defined between the two outer circles. The final contrast was then the difference between these two means. The gain was raised so the mean value of the signal in the anechoic cylinder was greater than zero.

Signal strength measurements were also made using the contrast detail test object. A uniform speckle region in the test object was averaged at each range sample location to determine signal strength through the paddles, with and without beamforming correction factors, relative to signal strength with no paddle. A fourth degree-polynomial fit was applied as a function of depth to reduce errors caused by noise.

Human Subject Scans

Informed consent was obtained using a protocol and other procedures that were approved by the Institutional Review Board. Women recruited for this study had clinically confirmed simple cysts. Strongly hypoechoic cysts were chosen for this study because they allowed quantitative and subjective measurements of ultrasound image quality losses due to the mammographic paddles that would affect detection and diagnosis of more complex solid masses.

To maximize comfort and minimize human subject motion during clinical scans, subjects were seated while the mammogram and ultrasound images were acquired. At the beginning of the procedure, a radiologist conducted a hand-held, direct-contact ultrasound scan across the breast to verify the region-of-interest (ROI) and determine the appropriate imaging view (cranial-caudal (CC), medial-lateral (ML), or mediolateral-oblique (MLO)). An acoustic coupling material was then placed between the transducer and paddle, and another was placed between the paddle and breast. Coupling between the transducer and paddle was achieved using water (contained in the paddle if the scan was in the CC view) or ultrasound gel (for LM/ML or LMO/

MLO views). The appropriate acoustic coupling material between the paddle and breast must prevent breast slippage (measured by subtracting an image taken at the end of the procedure from one taken at the beginning over the same plane) without creating bubbles or extra attenuation compared to traditional coupling aids. Based on these requirements, mineral oil, ultra-myossage lotion, glycerin and “sticky” primrose oil were individually tested for preliminary evaluation. The success of these and other coupling materials will be quantified and discussed in future studies.

After coupling materials were applied, the subject’s breast was compressed by the combined system and a foam wedge or a soft mammopad was placed underneath it to lift up the areolar region to improve anterior breast contact with the paddle. The transducer was then translated over the paddle and breast to obtain a whole breast volume. Afterwards, the ultrasound scan, the transducer, its carriage, and the coupling medium were removed from the compression paddle and a mammogram was taken. An appropriate filter was added to the mammography unit prior to imaging to account for differences in x-ray dose absorption between the tested paddle and the standard mammography paddle.

Contrast and CNR between tissue and cyst signal levels were calculated for each of the 10 human subjects scanned in this study using the equation:

$$CNR = \frac{\mu_{cyst} - \mu_{background}}{\sqrt{\sigma_{cyst}^2 + \sigma_{background}^2}} \approx \frac{contrast}{\sigma_{background}} \quad (2)$$

Based on the results from the test object experiments, human subject scans were performed through TPX 0.25 mm, 1.0 mm, or 2.5 mm paddles. System settings were adjusted to provide the clearest cyst images in the direct-contact ultrasound scan. The system gain was then increased to raise cyst signal level above zero to avoid underestimation of contrast between the background and the cyst. This did not change contrast measurements, however, because a linear grayscale map was used in all experiments. Additionally, saturation of the surrounding tissue signal was prevented by using a 72 dB display dynamic range. Gain was further increased between direct-contact and through-paddle scans to compensate for average signal loss through the paddle over the 4 cm depth, as determined by the test object experiments. Signal in the cyst ROI to within 1 mm of the cyst’s edge was compared with signal from ROIs in adjacent fat and glandular tissue, for both through-paddle and direct-contact scans. Log-decompressed signals were averaged over five slices in the ROIs.

Two radiologists evaluated the differences in clinical automated and hand scans in terms of overall image quality, ease of lesion detectability and relative image quality.

Results and Discussion

Spatial Resolution

Mean FWHM and FWTM values were calculated over a 4 cm depth range for each direction, with and without a paddle.

One exemplary plot of the elevational LSF is shown in Figure 3a. Mean FWHM values in the elevational direction for no paddle, TPX 2.5 mm paddle and lexan 375 μm paddle were 0.90 +/− 0.17 mm, 1.05 +/− 0.18 mm and 0.99 +/− 0.18 mm, respectively. Note that these values are within one standard deviation of each other and of no paddle values. Mean FWTM values were 2.10 +/− 1.0 mm, 2.56 +/− 1.2 mm and 2.18 +/− 1.1 mm, respectively. Mean sidelobe levels were calculated for each of the paddles relative to maximum signal level. With no paddle, the mean sidelobe level was −19.4 dB. Sidelobe levels were moderately elevated by paddles,

with TPX performing slightly better than lexan (−16.2 dB and −15.3 dB, respectively). Defocusing due to refraction and reverberations in the paddle caused image quality losses in the elevational direction.

Lengthening of the LSF as the beam travels through the paddle was inevitable, but could be reduced by implementing beamforming corrections. The improvement of image quality due to these corrections was most notable in the lateral direction, as expected. Figure 3b shows the lengthening of the LSF due to the TPX 2.5 mm paddle and its subsequent shortening when the corrections were applied.

Mean lateral FWHM and FWTM values for no paddle, TPX 2.5 mm and lexan 375 μm paddles without corrections were 0.39 ± 0.04 mm, 0.41 ± 0.04 mm and 0.41 ± 0.04 mm, respectively, and 0.70 ± 0.07 mm, 0.75 ± 0.09 mm and 0.90 ± 0.14 mm, respectively. A student t-test revealed that even without beamforming corrections, the differences in FWHM were not statistically significant, though the differences in FWTM were. With corrections, the TPX 2.5 mm and lexan 375 μm mean FHWM and FWTM values reduced to 0.40 ± 0.02 mm and 0.40 ± 0.03 mm, and 0.72 ± 0.04 and 0.81 ± 0.12 mm, respectively. Thus, the addition of the TPX and lexan paddles only caused a 5% increase in lateral FWHM values, which was reduced to a 2% increase after beamforming corrections were implemented. Lateral FWTM values increased 28.5% due to the lexan paddle but only 7% due to the TPX paddle without corrections, and to 17% and 3%, respectively, with corrections.

Pulse lengthening due to the paddle was practically negligible in the axial direction and, thus, beamforming correction improvements in this direction were also negligible (Figure 4a). Before correction algorithms were implemented, no paddle, TPX 2.5 mm paddle and lexan 375 μm paddle mean FWHM and FWTM values were 0.23 ± 0.03 mm, 0.23 ± 0.03 mm and 0.25 ± 0.03 mm, respectively and 0.48 ± 0.04 mm, 0.48 ± 0.04 mm and 0.55 ± 0.04 mm, respectively. After beamforming corrections were applied, TPX 2.5 mm paddle and lexan 375 μm paddle mean FWHM and FWTM values reduced to 0.22 ± 0.02 mm and 0.24 ± 0.02 mm and 0.46 ± 0.02 mm and 0.54 ± 0.03 mm, respectively.

In the axial direction, the addition of substantial range lobes can significantly degrade an image. As range lobes increase, they affect the main lobe, degrading resolution. When no paddle was present, the impulse response of the transducer produced range lobes −39 ± 3.1 dB from the signal maximum, averaged over 1.5 to 3.2 cm depths. They were visibly increased with the lexan paddle (−29 ± 5.2 dB) and marginally increased by the TPX paddle (−37 ± 4.9 dB) when beamforming corrections were not implemented (Figure 4b). The high range lobe levels of the lexan paddle were caused by its high impedance mismatch with saline ($z = 1.48\ kg/m^2s$). Implementation of beamforming corrections reduced TPX range lobes to −40 ± 3.5 dB and lexan range lobes to −30 ± 3.3 dB. No signal difference was observed between paddles and no paddle beyond 2 mm of the main signal lobe, confirming that all reverberations were included in the range lobe response. Because both paddles exhibit range lobe levels ≥ 30 dB down from signal maximum, range lobes should not be a major concern for this system.

All LSF measurements, with beamforming corrections implemented where relevant, are summarized in Table 2.

Contrast

Object contrast was calculated as a function of depth with beamforming corrections implemented (Figure 5a). Averaged over 25 mm to 36 mm, the contrast of the anechoic cylinder was −23 dB, −20 dB and −20 dB, respectively, for no paddle, TPX 2.5 mm paddle and lexan 375 μm paddle. Valleys in these plots are at transitions between transmit focal zones. Overall, contrast decreases with depth, mainly due to increased signal loss, beam degradation, and

accumulation of multiple scattering as the beam propagates further into tissue. This reinforces the importance of positioning breast lesions as close to the transducer as possible for high contrast, and thus high quality, ultrasound images. Mean contrast values for each paddle and no paddle are listed in Table 2.

Relative Signal Strength

Figure 5b shows relative signal strength for the TPX and lexan paddles over common breast lesion depths. Signal loss through the paddles occurred in the form of beam absorption and reflection. At depths greater than 3.2 cm, acoustic and electronic noise caused a minor rise in relative signal loss. The TPX paddle exhibited less signal loss averaged over the 4 cm range than the lexan paddle (−6 dB and −8.3 dB, respectively), despite being 6 times thicker. These values are listed in Table 2.

Evaluation of TPX Paddles < 2.5 mm

Image performance of thinner TPX paddles (250 μm and 1.0 mm) was also compared with TPX 2.5 mm results. These thinner paddles exhibited similar LSF and contrast values as the 2.5 mm paddle, but with less signal loss (−2.4 dB and −4.2 dB, respectively). When less signal loss or a more flexible paddle is preferred, these paddles could also be used for mammographically compatible ultrasound. Even so, thin paddles exhibit greater deformation than thicker paddles, which results in a non-planar scan surface for the ultrasound probe. This trade-off between signal loss and paddle deformation can be decided according to system design and requirements.

Summary of Test Object Results

Overall, imaging through a mammographic paddle only mildly degraded test object image quality when beamforming corrections were implemented. Compared with no paddle values, LSF FWHM calculated through paddles increased 10% (lexan 375 μm paddle) and 17% (TPX 2.5 mm paddle) in the elevational direction and ≤ 5% in the lateral and axial directions for both paddles. Sidelobe levels were increased ≤ 4 dB regardless of paddle material and range lobe levels were comparable between no paddle and the TPX 2.5 mm paddle, but increased 9 dB with the lexan 375 μm paddle. Signal loss was 8 dB greater through the lexan paddle than through no paddle, but only 6 dB greater through the TPX paddle even though it was 6 times thicker than the lexan paddle. A summary of all these image quality measurements is listed in Table 2.

Based on these results, it is clear that the TPX 2.5 paddle performed better than the lexan 375 μm paddle overall and the minor losses in image quality through this paddle should not inhibit detection or characterization of lesions. To determine whether these losses had a clinical impact, we compared cyst contrast, lesion detectability, and overall image quality with and without a mammographic paddle in human subjects, as described below.

Human Subject Scans

Before high quality images can be obtained with the combined system, adequate human subject positioning, acoustic coupling, and breast stabilization must occur. Though these topics will be addressed more thoroughly in future studies, preliminary efforts to stabilize and sonographically image the breast through the paddle will be briefly mentioned here.

Stable positioning of the compressed breast is crucial to ensure efficient scanning procedures, complete breast coverage, and accurate registration of ultrasound and mammographic images. If the human subject's breast begins to slip during the procedure, the paddle will lose contact with parts of the breast and important structural information will be lost. The breast might then

need to be removed from compression and repositioned, contributing to human subject procedure time.

Adding a Mammopad under the breast helped prevent it from sliding during compression, and human subjects find the soft material comfortable. Foam wedges used to push the areolar region upward towards the paddle were partially successful at improving imaging of anterior breast tissue. Ultrasound gel and water have successfully coupled the transducer to the paddle, allowing it to scan across the paddle without interruptions in coupling contact, though water is more easily applied and removed. However, none of the coupling materials (mineral oil, ultra-myossage lotion, glycerin, or "sticky" primrose oil) were able to keep the breast in the same position at the end of the scan as at the beginning. Future work will include investigating better coupling materials for this purpose.

Though these methods of coupling and stabilization were not necessarily ideal, they were sufficient to obtain preliminary human subject images of simple cysts which could be compared to the image quality of direct-contact scans.

Treating the human subject cysts as ellipsoids, mean areas in automated, through-paddle and hand-held, direct-contact scans were 150 ± 140 mm^2 and 190 ± 160 mm^2, respectively. Differences in apparent cyst size were most likely caused by alteration of the cyst's shape in the third dimension during compression. Mean depths of the centers of the cysts in the two scan modes were 19 ± 1.8 and 18 ± 3.0 mm. There was no distinguishable correlation between contrast and cyst depth because cyst depths were so similar.

In through-paddle and direct-contact scans, average signal levels were: cyst −68 and −69 dB; fat −52 and −52 dB; and glandular −45 and −44 dB, respectively. This indicates that the contrast in through-paddle and direct-contact was 14 ± 10 and 16 ± 9 dB, respectively, between fat tissue and cyst and 25 ± 21 and 27 ± 23 dB, respectively, between glandular tissue and cyst (Figure 6a, b). The ~1.5 − 2.0 dB loss in contrast for both types of tissue is slightly less than the 3 dB contrast loss calculated in the test object scans averaged over a 4 cm depth, because human subject contrast was calculated only at cyst levels. In six out of 10 human subjects, hand-held, direct-contact fat-to-cyst contrast was greater than automated, through-paddle fat-to-cyst contrast. In four out of six human subjects in which substantial glandular signal could be identified at the same depth as the cyst, direct-contact cyst-to-glandular-tissue contrast was greater than through-paddle cyst-to-glandular-tissue contrast. Cyst-to-fat CNR for through-paddle and direct-contact scans was 5.5 ± 3.0 and 7.5 ± 3.6, respectively, and cyst-to-glandular tissue CNR was 9.8 ± 1.3 and 10.0 ± 2.0, respectively. This data was not statistically significant because of the small size of the group. In every case for both scan modes, cyst signal levels were lower than fat signal levels, which were lower than glandular signal levels.

Contrast and CNR losses can be expected from multiple scattering, discrete reverberations, and clutter in the region of the cyst. These factors will increase the noise signal level in the cyst, decreasing contrast and CNR values. Specifically, cyst fill-in can be caused by multiple scatterers acting in the axial direction proximal to the anechoic cysts (Carson and Oughton 1977). Cysts larger than 200 mm^2 exhibited visible fill-in, whereas smaller cysts appeared to be hypoechoic throughout their entire area. Radiologist interpretations were that the moderate fill-in did not obstruct recognition of the cyst as long as it mostly remained hypoechoic. Multiple scattering effects contributing to cyst fill-in could further be minimized by employing a lower frequency transducer during scans. A t-test performed on contrast and CNR values gave a p-value > 0.1 in both cases, indicating that differences in through-paddle and direct-contact contrast and CNR were not statistically significant.

To determine whether these minor losses had a clinical impact, two radiologists were asked to blindly evaluate six randomly chosen, corresponding automated, through-paddle and hand-

held, direct-contact scans according to overall image quality and lesion detectability. Images created by both scan types were presented in cineloop format. Of 12 ratings of six cases, the radiologists ranked overall image quality of the through-paddle scans equal to or better than their corresponding direct-contact scan in 83% of the cases. In terms of ease of lesion detectability, the through-paddle scan was rated equal to or better than the direct-contact scan in 75% of the cases. Additionally, the radiologists ranked the image quality of scans individually on a scale from 1–5, with a score of "1" corresponding to "poor" and a score of "5" corresponding to "excellent". The mean rating for the through-paddle images was 3.3 and the mean rating for the radiologist performed direct-contact images was 3.0. Having the automated-through paddle scans sampled finely and uniformly throughout the imaged volumes may have contributed to their perceived higher image quality. Table 3 summarizes *in vivo* image quality comparisons of direct-contact and through-paddle images. These results further validate that minor image quality losses observed with this system will not impair detection or characterization of cystic lesions.

Conclusions

The combined system with stable breast compression promises to utilize the synergism between ultrasound and x-ray mammography for more accurate and efficient breast lesion examination. Advanced features such as elasticity imaging, vascular imaging, and tomosynthesis may further increase our ability to discriminate between benign and malignant lesions, as well as to detect changes in lesions over extended periods.

Among those tested, the TPX paddle was judged best overall for ultrasound and mammographic imaging requirements. FWHM and FWTM values in the elevational direction were within 17% of no paddle values and, in lateral and axial directions, were within 5% of no paddle values when beamforming corrections were implemented. These corrections were critical in maintaining resolution levels very close to no paddle values, particularly in the lateral direction and for thicker paddles.

Range lobes due to the TPX paddle were comparable or modestly increased relative to no paddle levels (37 to 40 dB down from maximum signal level). Range lobes can be further minimized by choosing an impedance-matched material. The 6 dB pulse echo signal strength loss due to beam attenuation and reflection through the TPX 2.5 paddle is minor compared with the full dynamic range (72 dB) of gray-scale images and could be reduced by imaging through a thinner paddle, such as TPX 0.25 mm or 1.0 mm, at the expense of additional paddle deformation.

Human subject movement, comfort and examination time remain targets for further effort with the system. Additional coupling materials should be explored, as well as mechanical alternatives, such as tilting the compression paddle to image closer to the chest wall. A hollow wedge rather than a foam wedge might hold the areolar region of the breast against the paddle well enough to provide adequate contact for anterior breast imaging.

Cysts and lesions near the chest wall are still difficult to image because of the rigid wall of the compression paddle and the designs of the transducer housing and carriage. Imaging in trapezoidal (virtual convex) mode or beam steering at ±20° somewhat alleviates this problem by electronically steering the transducer to image regions-of-interest that would not be seen in a rectangular scan. Though not quantified, the initial images created using these formats (Figure 7) suggest high image quality can be maintained through TPX paddles.

With the combined system, small relative contrast and CNR loss *in vivo* is possibly from increased reverberation and multiple scattering signals, LSF degradation and signal loss in the paddle, all of which can be seen in the hypoechoic cysts. These minor contrast losses are

approximately consistent with the signal loss (~6 dB) and increased range lobe levels (~2 dB) measured when imaging line targets through the compression paddles. Half the signal loss through the paddles can be compensated for, with no increased ultrasound exposure levels to the human subject, by increasing the power transmitted into the breast to the levels that would have existed with no paddle. In subjective assessments, minor image quality losses did not affect interpretations by radiologists, reinforcing our belief that the losses in these scans do not have an adverse clinical impact. These minor losses may well be worth the many advantages of 3D, whole breast automated ultrasound scanning and co-registered mammography.

Acknowledgements

This work was supported in part by NIH grant RO1 CA 091713.

References

Bassett LS, Kimme-Smith C. Breast Sonography. AJR 1991;156:499–455.

Brem RF, Gatewood OMB. Template-guided breast US. Radiology 1992;184:872–874. [PubMed: 1509083]

Carson PL, Oughton TV. A modeled study for diagnosis of small anechoic masses with ultrasound. Radiology 1977;122(3):765–71. [PubMed: 841069]

Conway WF, Hayes CS, Brewer WH. Occult breast masses: Use of mammographic localizing grid for US evaluation. Radiology 1991;181:143–146. [PubMed: 1653441]

Department of Health and Human Services, Food and Drug Administration. Mammography quality standards final Rules. Federal Register Oct 28;1997 68(208):55852–55994.

Hoctor, RT.; Thomenius, KE. Focus Correction for Ultrasound Imaging Through Mammography Compression Plate. US Patent No. 6,607,489. Aug. 19. 2003

Jackson VP. The role of US in breast imaging. Radiology 1990;177:305–311. [PubMed: 2217759]

Jackson VP, Hendrick RE, Reig SA, Kopans DB. Imaging of the radiographically dense breast. Radiology 1993;188(2):297–301. [PubMed: 8327668]

Kapur A, Carson PL, Eberhard J, et al. Combination of digital mammography with semi-automated 3D breast ultrasound. Technol Cancer Res Treat 2004 Aug;3(4):325–334. [PubMed: 15270583]

Kelly-fry E, Jackson VP. Adaptation development and expansion of x-ray mammography techniques for ultrasound mammography. Ultrasound Med 1991;10:S-16.

Kolb TM, Lichy J, Newhouse JH. Occult cancer in women with dense breasts: Detection with screening ultrasound: Diagnostic yield and tumor characteristics. Radiology 1998;207:191–198. [PubMed: 9530316]

Krücker JF, Fowlkes JB, Carson PL. Sound speed estimation using automatic ultrasound image registration. IEEE Trans Ultrason Ferroelectr Freq Control 2004;51(9):1095–1106. [PubMed: 15478971]

Lister D, Evans AJ, Burrell HC, et al. The accuracy of breast ultrasound in the evaluation clinically benign discrete, symptomatic breast lumps. Clin Radiology 1998;53:490–492.

Moskalik AP, Carson PL, Meyer CR, Fowlkes JB, Rubin JM, Roubidoux MA. Registration of three-dimensional compound ultrasound scans of the breast for refraction and motion correction. Ultrasound in Med and Biol 1995;21(6):769–778. [PubMed: 8571465]

Moss HA, Britton PD, Flower CDR, Freeman AH, Lomas DJ, Warren RML. How reliable is modern breast imaging in differentiating benign from malignant breast lesions in the symptomatic population? Clinical Radiology 1999;54:676–682. [PubMed: 10541394]

Novak D. Indications for and comparative diagnostic value of combined ultrasound and x-ray mammography. Eur J Rad 1983;3 (Suppl 1):299–302.

Richter K. Technique for detection and evaluating breast lesions. Ultrasound Med 1994;13:797–802.

Richter K. Clinical amplitude/velocity reconstructive imaging (CARI): A new sonographic method for detecting breast lesions. BR J Radiol 1995;68:375–384. [PubMed: 7795973]

Richter K, et al. Detection of malignant and benign breast lesions with an automated US system: results in 120 cases. Radiology 1997;205:823–830. [PubMed: 9393543]

Schütze B, Marx C, Fleck M, Reichenbach J, Kaiser WA. Diagnostic evaluation of sonographically visualized breast lesions by using a new clinical amplitude/velocity reference imaging technique (CARI sonography). Invest Radiol 1998;33:341–347. [PubMed: 9647446]

Stavros AT, Thickman D, Rapp CL, Dennis MA, Parker SH, Sisney GA. Solid breast nodules: Use of sonography to distinguish between benign and malignant lesions. Radiology 1995;196:123–134. [PubMed: 7784555]

Taylor KJW, Merritt C, Piccoli C, et al. Ultrasound as a complement to mammography and breast examination to characterize breast masses. Ultrasound in Med and Biol 2002;28(1):19–26. [PubMed: 11879948]

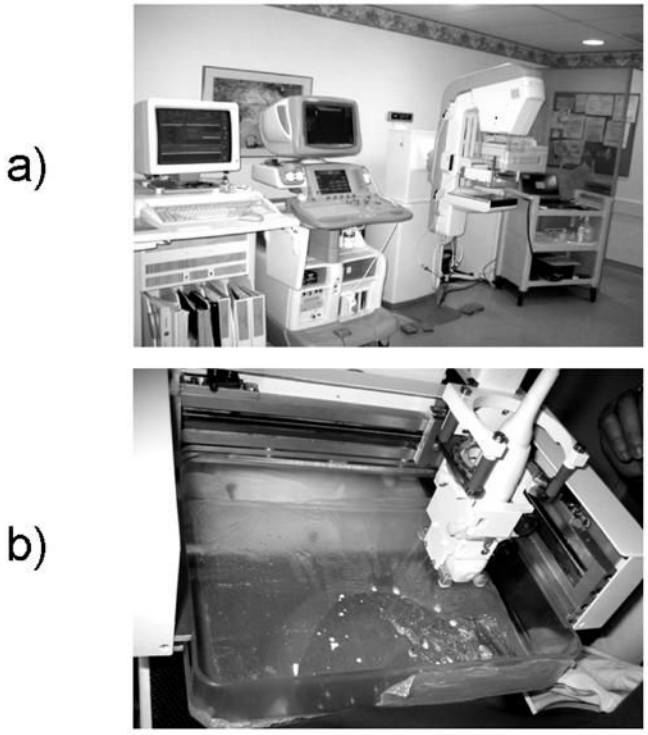

Fig 1.

a) Combined 3D ultrsound/digital mammography system. From left to right are the mammogram storage unit, GE Logiq 9 scanner, Senographe 2000D digital mammography unit, and cart containing hardware and software to drive the combined system. b) Close up view of a breast compressed between the mammographic paddle and x-ray detector, with the ulrasound transducer and holder attached.

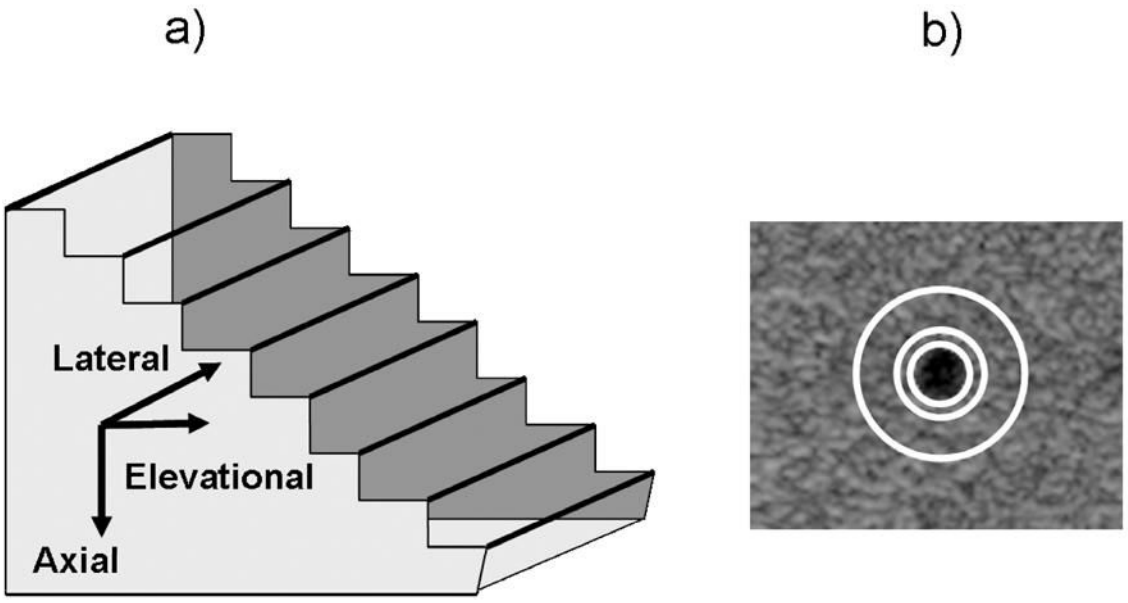

Fig 2.

a) Step-shaped string test object with 25 μm silver wires acting as line targets to assess the LSF of the system in all three directions. b) Anechoic cylinder within contrast test object for determining contrast with and without imaging through a mammographic paddle. Mean cylinder amplitude was calculated within the innermost white circle and mean background amplitude was calculated in the area between the two outermost white circles. Mean signal strength for each paddle and no paddle was also calculated from a uniform speckle region within this phantom over a 4 cm depth.

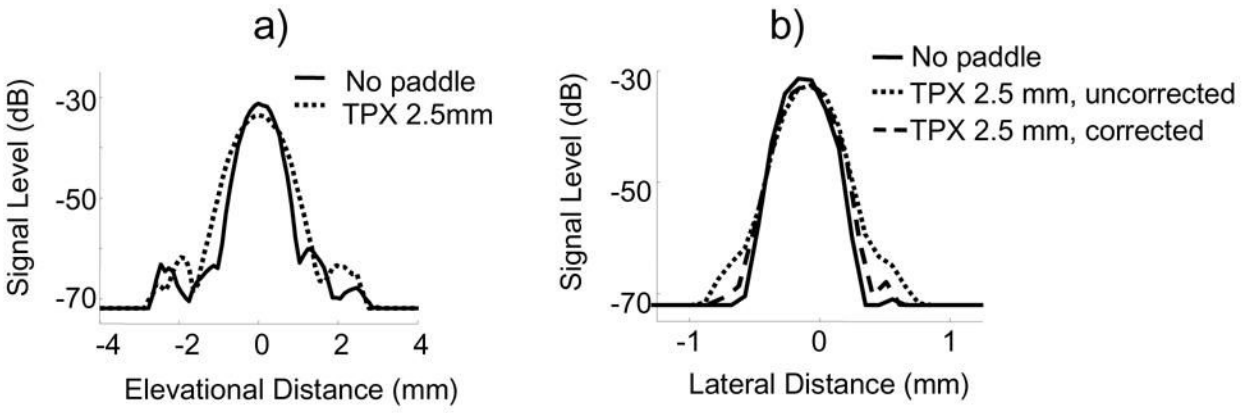

Fig 3.

Representative a) elevational LSF and b) lateral LSF for no paddle and TPX 2.5 mm paddle. Lexan 375 μm paddle LSFs exhibited similar shapes to no paddle LSFs. Lateral LSF was calculated with and without beamforming corrections. In the elevational direction, FWHM values were increased up to 17% and sidelobe levels were increased up to 4 dB when imaging through a paddle. FWHM values in the lateral direction were only increased 2% in both paddles when beamforming corrections were implemented.

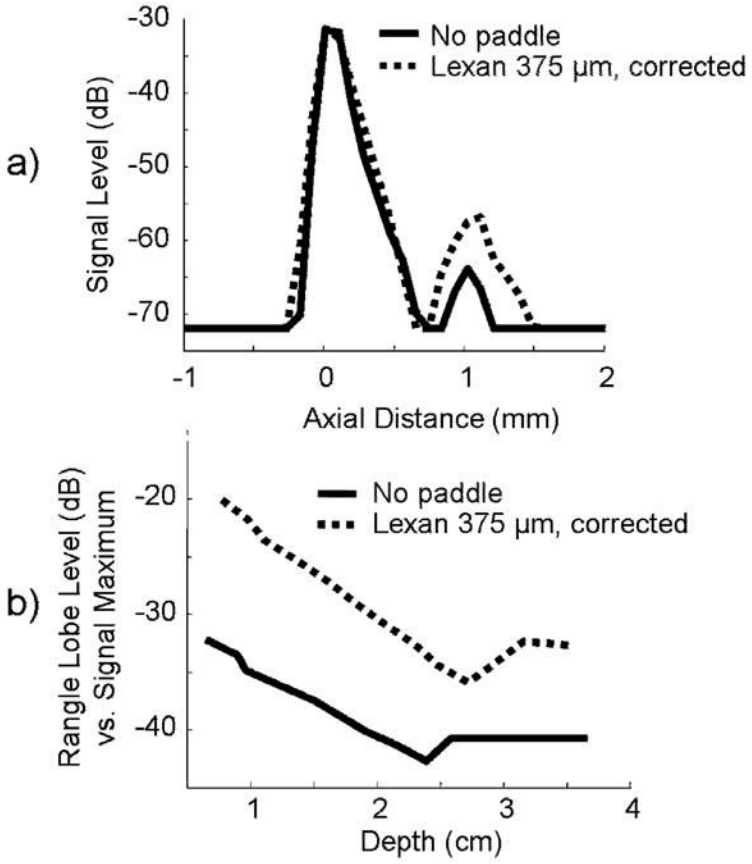

Fig 4.

a) Axial LSF and b) relative range lobe levels for no paddle and lexan 375 µm paddle with beamforming corrections. Range lobe levels, which include all reverberations, were 9 dB greater when imaging through the lexan paddle than when imaging through the TPX paddle or no paddle, primarily due to the acoustical impedance mismatch between lexan and saline.

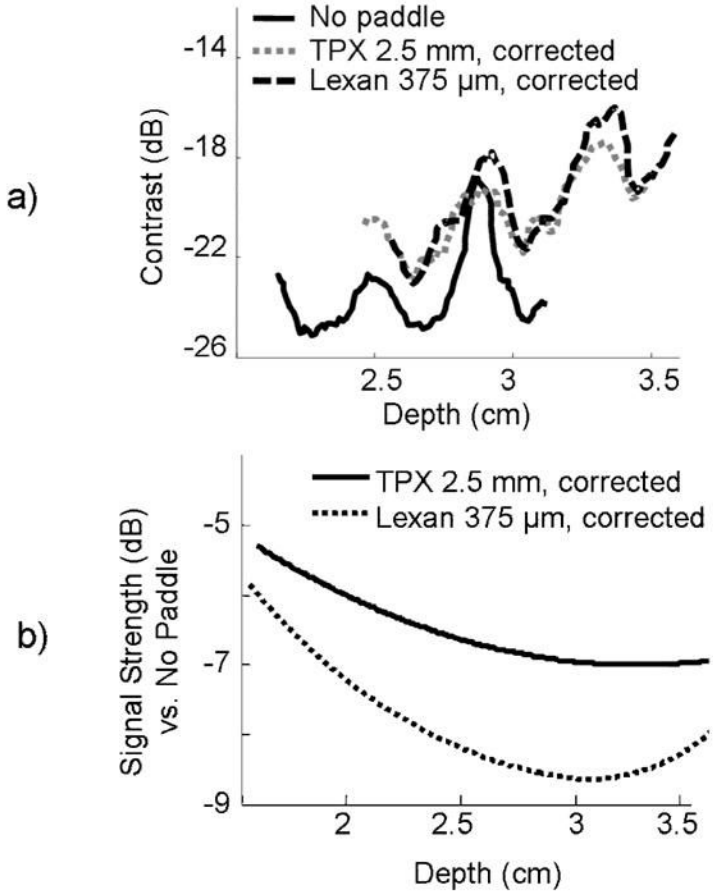

Fig 5.

a) Contrast between a small anechoic cylinder (mimicking a simple cyst) lying orthogonal to the image plane and a uniform speckle background, shown as a function of depth for TPX and lexan paddles, and no paddle. Contrast decreases with depth as the ultrasound beam is attenuated. Valleys correspond to transitions between transmit focal zones. b) Signal strength compared to no-paddle, with beamforming corrections over common breast imaging depths. TPX is clearly a much less acoustically attenuating material than lexan.

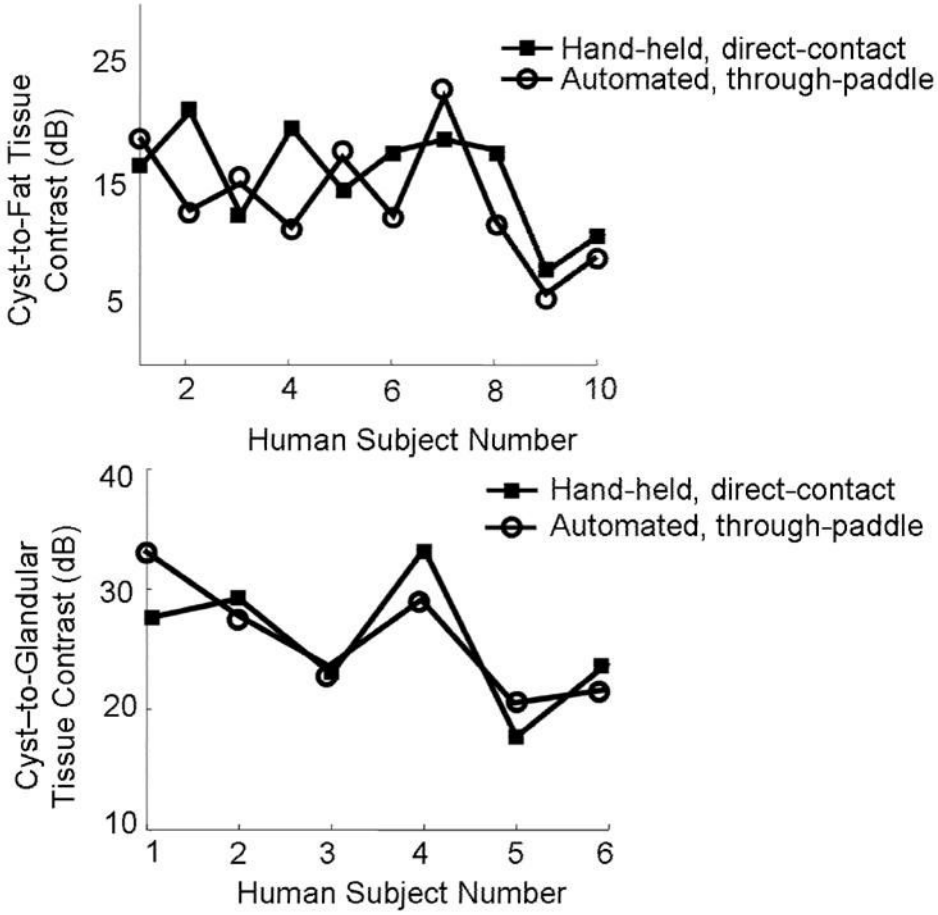

Fig 6.

a) Cyst-to-fat contrast in 10 human subjects with simple cysts. b) Cyst-to- glandular contrast for the six human subjects whose breasts contained enough glandular tissue for measurement. Contrast levels in both cases were similar, and small differences proved to be statistically insignificant.

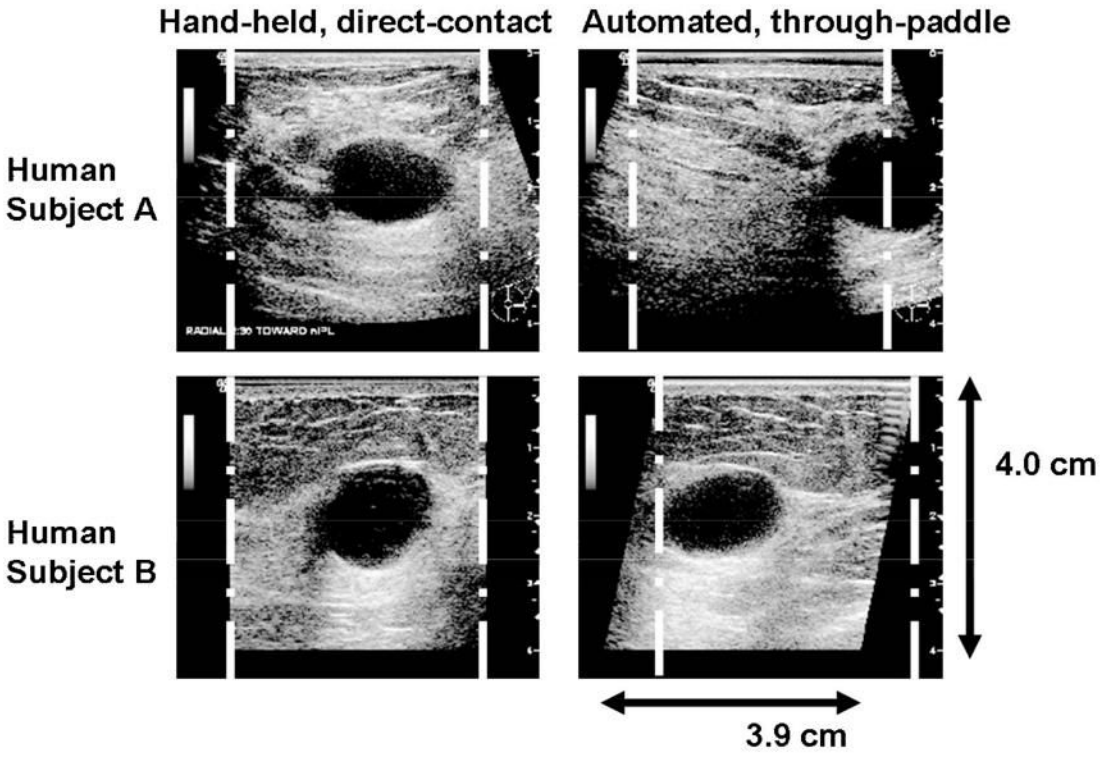

Fig 7.

Human subject A: (left) hand-held, direct contact scan of cyst and (right) automated, through-paddle scan of cyst, both in trapezoidal (virtual convex) mode. Human subject B: (left) hand-held, direct-contact scan and (right) automated, through-paddle scan with 20° beam steering. White lines indicate the image region of a rectangular scan mode. Changing to different scan modes increases lesion visibility close to the chest wall, which might otherwise be obstructed due to imaging through a rigid mammographic paddle.

Table 1

Acoustic properties of mammograhic paddles. * **

Paddle	Speed of Sound (mm/μs)	Attenuation (dB/cm/MHz)	Acoustical impedance (kg/(m^{2}s))
TPX	2.22	1.1	1.84
Lexan	2.30	4.6	2.75

* Physical properties can vary substantially with the specific formulation of the polymer.

** Source: Onda Corporation, “Acoustic Properties of Plastics”

Table 2

Image quality summary based on test object experiments for no paddle, TPX 2.5 mm paddle and lexan 375 μm paddle. Beamforming corrections were implemented on all relevant measurements.

Paddle	No paddle	TPX 2.5 mm	Lexan 375 μm
Elevational FWHM (mm)	0.90 +/− 0.17	1.05 +/− 0.18	0.99 +/− 0.18
Elevational FWTM (mm)	2.1 +/− 1.0	2.6 +/− 1.2	2.2 +/− 1.1
Mean sidelobe level (dB)	−19.4	−16.2	−15.3
Lateral FWHM (mm)	0.39 ± 0.04	0.40 ± 0.02	0.40 ± 0.03
Lateral FWTM (mm)	0.70 ± 0.07	0.72 ± 0.04	0.81 ± 0.12
Axial FWHM (mm)	0.23 ± 0.03	0.22± 0.02	0.24 ± 0.02
Axial FWTM (mm)	0.48 ± 0.04	0.46 ± 0.02	0.54 ± 0.03
Range lobe levels (dB)	−39 ± 3.1	−40 ± 3.5	−30 ± 3.3
Contrast (dB)	−23	−20	−20
Average signal strength vs. no paddle (dB)	0	−6.0	−8.3

Table 3

Quantitative and qualitative comparison of hand-held, direct-contact vs. automated, through-paddle *in vivo* ultrasound scans of 10 women with simple cysts.

	Percentage of through-paddle ≥ direct-contact images
Cyst-to-fat tissue contrast	60%
Cyst-to-glandular tissue contrast	67%
Lesion detectability	75%
Overall image quality	83%